



HAL
open science

Optimization of a coaxial electron cyclotron resonance plasma thruster with an analytical model

F. Cannat, T. Lafleur, J. Jarrige, P Chabert, P.Q. Elias, D. Packan

► **To cite this version:**

F. Cannat, T. Lafleur, J. Jarrige, P Chabert, P.Q. Elias, et al.. Optimization of a coaxial electron cyclotron resonance plasma thruster with an analytical model. *Physics of Plasmas*, 2015, 22 (5), p. 053503 (12 p.). 10.1063/1.4920966 . hal-01229071

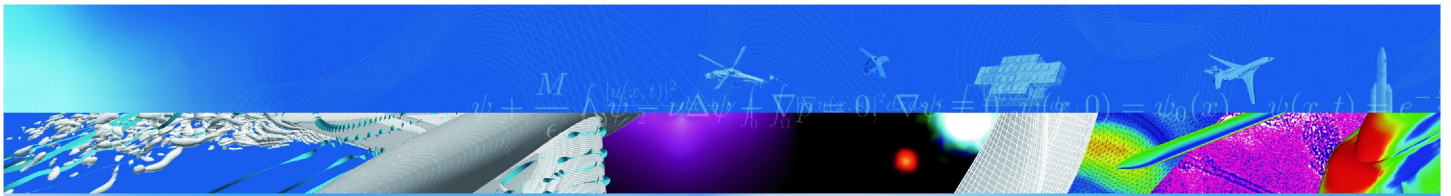
HAL Id: hal-01229071

<https://hal.science/hal-01229071>

Submitted on 16 Nov 2015

HAL is a multi-disciplinary open access archive for the deposit and dissemination of scientific research documents, whether they are published or not. The documents may come from teaching and research institutions in France or abroad, or from public or private research centers.

L'archive ouverte pluridisciplinaire **HAL**, est destinée au dépôt et à la diffusion de documents scientifiques de niveau recherche, publiés ou non, émanant des établissements d'enseignement et de recherche français ou étrangers, des laboratoires publics ou privés.



T I R É À P A R T

Optimization of a coaxial electron cyclotron resonance plasma thruster with an analytical model

F. Cannat, T. Lafleur *, J. Jarrige, P. Chabert *,
P.Q. Elias, D. Packan

PHYSICS OF PLASMAS
Vol. 22, pp. 053503 (12 pages)

TP 2015-244



r e t o u r s u r i n n o v a t i o n

Optimization of a coaxial electron cyclotron resonance plasma thruster with an analytical model

Optimisation d'un propulseur plasma coaxial à résonance cyclotronique des électrons avec un modèle analytique

par

F. Cannat, T. Lafleur *, J. Jarrige, P. Chabert *, P.Q. Elias, D. Packan

* Ecole Polytechnique, Palaiseau, France

Résumé traduit :

Un nouveau propulseur plasma sans cathode actuellement en développement à l'Onera est présenté et caractérisé expérimentalement et analytiquement. Le propulseur coaxial consiste à une antenne immergée dans un champ magnétique pour chauffer les électrons par résonance. Le champ magnétique est divergent et forme une tuyère magnétique qui accélère un plasma quasi-neutre pour générer la poussée. Différentes configurations du propulseur ont été testées et en particulier l'influence du diamètre sur les performances du propulseur est investiguée. Pour une puissance micro-onde de 30 W et un débit de xénon de 0.1 mg/s, une utilisation massique de 60 % et une poussée de 1 mN est estimée avec des mesures de courant angulaires à l'aide de sondes électrostatiques. Les résultats trouvés sont très proches d'un modèle analytique initialement adapté pour un propulseur Helicon.

Optimization of a coaxial electron cyclotron resonance plasma thruster with an analytical model

F. Cannat, T. Lafleur, J. Jarrige, P. Chabert, P.-Q. Elias, and D. Packan

Citation: *Physics of Plasmas* (1994-present) **22**, 053503 (2015); doi: 10.1063/1.4920966

View online: <http://dx.doi.org/10.1063/1.4920966>

View Table of Contents: <http://scitation.aip.org/content/aip/journal/pop/22/5?ver=pdfcov>

Published by the [AIP Publishing](#)

Articles you may be interested in

[Waveguide slot-excited long racetrack electron cyclotron resonance plasma source for roll-to-roll \(scanning\) processing](#)

Rev. Sci. Instrum. **84**, 073513 (2013); 10.1063/1.4815822

[Internal plasma potential measurements of a Hall thruster using plasma lens focusing](#)

Phys. Plasmas **13**, 103504 (2006); 10.1063/1.2358331

[Internal plasma potential measurements of a Hall thruster using xenon and krypton propellant](#)

Phys. Plasmas **13**, 093502 (2006); 10.1063/1.2335820

[Physical characterization of high-frequency instabilities in Hall thrusters](#)

Phys. Plasmas **13**, 083503 (2006); 10.1063/1.2231723

[Magnetically filtered Faraday probe for measuring the ion current density profile of a Hall thruster](#)

Rev. Sci. Instrum. **77**, 013503 (2006); 10.1063/1.2149006



PFEIFFER VACUUM

VACUUM SOLUTIONS FROM A SINGLE SOURCE

Pfeiffer Vacuum stands for innovative and custom vacuum solutions worldwide, technological perfection, competent advice and reliable service.

125 YEARS NOTHING IS BETTER

Optimization of a coaxial electron cyclotron resonance plasma thruster with an analytical model

F. Cannat,^{1,2,a)} T. Lafleur,^{1,2} J. Jarrige,¹ P. Chabert,² P.-Q. Elias,¹ and D. Packan¹

¹Physics and Instrumentation Department, Onera -The French Aerospace Lab, Palaiseau, Cedex 91123, France

²Laboratoire de Physique des Plasmas, CNRS, Sorbonne Universites, UPMC Univ Paris 06, Univ Paris-Sud, Ecole Polytechnique, 91128 Palaiseau, France

(Received 27 February 2015; accepted 29 April 2015; published online 8 May 2015)

A new cathodeless plasma thruster currently under development at Onera is presented and characterized experimentally and analytically. The coaxial thruster consists of a microwave antenna immersed in a magnetic field, which allows electron heating via cyclotron resonance. The magnetic field diverges at the thruster exit and forms a nozzle that accelerates the quasi-neutral plasma to generate a thrust. Different thruster configurations are tested, and in particular, the influence of the source diameter on the thruster performance is investigated. At microwave powers of about 30 W and a xenon flow rate of 0.1 mg/s (1 SCCM), a mass utilization of 60% and a thrust of 1 mN are estimated based on angular electrostatic probe measurements performed downstream of the thruster in the exhaust plume. Results are found to be in fair agreement with a recent analytical helicon thruster model that has been adapted for the coaxial geometry used here. © 2015 AIP Publishing LLC. [<http://dx.doi.org/10.1063/1.4920966>]

I. INTRODUCTION

The future of spacecraft propulsion systems will rely more and more heavily on electric thrusters. They achieve a higher specific impulse than classical chemical rockets and thus allow a drastic reduction in the mass of onboard propellant,¹ which translates into either an increase in the available payload or a reduction in launch costs. As a result, electric thrusters are receiving more and more attention, and new satellite platforms that use electric propulsion for both orbit transfer and station keeping are being developed by most satellite manufacturers (Boeing, Airbus Defence and Space, Thales).

The most mature electric thruster technologies, Hall Effect Thrusters and Gridded Ion Thrusters, are based on direct electrostatic acceleration of ions. They have already been used in space missions, such as Deep Space 1² or HAYABUSA,³ and are routinely used on large Telecom platforms for station keeping. Current research on these plasma thruster technologies focuses on specific issues such as instabilities, operating ranges, and extension of their lifetimes.^{4,5} In particular, the neutralizer, the grids, and the low thrust operation are areas of interest and challenge for these technologies. The neutralizer affects cost, reliability, and lifetime because of plasma erosion and sensitivity to gas impurities and thermal life cycles. Grids are also a cost and reliability issue for gridded thrusters because of ion erosion. Finally, Hall Effect and Ion Thrusters have a low efficiency in the μN and mN thrust range, whereas the small satellite market that would need these thrust levels is expected to grow in the future.⁶

In order to provide improvement over the existing technologies in these areas, the next generation of electric

thrusters is under development, and in particular, cathodeless plasma thrusters are attracting attention. Some cathodeless thrusters use grids (PEGASES⁷ and NEPTUNE⁸), others are based on the magnetic nozzle principle and can operate without electrodes. The latter are therefore cathodeless and potentially electrodeless. Such magnetic nozzle thrusters use a magnetic field to enhance the absorption of electric power in the plasma, to reduce particle losses on the walls by confinement, and/or to accelerate the plasma flow in a magnetic nozzle, thus providing a quasi-neutral and current-free plume.⁹ Two typical examples of cathodeless-electrodeless plasma thrusters are the Helicon Plasma Thruster (HPT)^{10,11} and the Electron Cyclotron Resonance (ECR) plasma thruster.^{12,13} They are based on the excitation of a plasma by radio-frequency (rf) waves. The difference between HPT and ECR thrusters comes from the mechanism of energy transfer to the plasma. Helicon plasma sources produce a high density plasma using frequencies in the MHz range.¹⁴ Power absorption occurs by inductive coupling from an rf antenna, and the excitation of resonance helicon waves within the plasma. In recent experiments, Takahashi *et al.* have obtained a high specific impulse of 2000 s with a thruster efficiency between 4% and 7%.¹⁵ In ECR plasma sources, a microwave field in the GHz range is used to heat the electrons by resonant absorption and to create a high density plasma. In the 1960s, two groups of researchers first investigated ECR plasma acceleration for its potential application to spacecraft propulsion: General Electric (USA)^{16,17} and the University of Tokyo (Japan).¹⁸ Their work has shown that a well-designed ECR system can couple over 95% of the incident microwave power into the plasma. Later in 1967, Kosmahl¹⁹ realized a first theoretical analysis of ECR plasma acceleration, showing that the propulsive efficiency depends primarily on the magnetic field topology and the position of

^{a)}Author to whom correspondence should be addressed. Electronic addresses: felix.cannat@onera.fr and felix.cannat@gmail.com

the ionization region. No further investigations on ECR thrusters were led at that time because the microwave sources were quite massive and inefficient for space propulsion and meanwhile the progress on electrostatic thrusters (Hall Effect and Gridded Ion thruster) was significant and provided acceptable performance. Later in the 1990s, further work on ECR plasma thrusters was performed at the California Institute of Technology.²⁰ In particular, the work of Sercel led to the conclusion that the measurement of power efficiency was limited by the effects of the vacuum background pressure (which are well known to play an important role in the experimental testing of electric propulsion systems²¹), wall losses on the thruster, and the poor magnetic nozzle efficiency. Experimental results indicated 85% mass utilization efficiency, 30% power efficiency, and 24% of divergence factor efficiency. Currently, several research groups work on the cyclotron resonance thruster concept. One of them is the Plasmadynamics & Electric Propulsion Laboratory at the University of Michigan with the Gasdynamic Mirror (ECR-GDM)²² for high thrust generation. The ECR-GDM has a magnetic mirror confinement system to heat the propellant by electron cyclotron resonance for a period of time and then accelerate the plasma with a magnetic nozzle to produce thrust. Another group working on cyclotron resonance, the Ad Astra Rocket Company, uses Ion resonance instead of Electron resonance (ICR instead of ECR), and has designed the high powered Variable Specific Impulse Magnetoplasma Rocket, or VASIMR[®]. The VASIMR thruster consists of a helicon plasma source that produces a high density plasma, followed by an ion cyclotron resonance booster stage, and eventually a magnetic nozzle to accelerate the plasma.^{23,24}

The Physics and Instrumentation Department at Onera is currently performing research on an ECR plasma thruster that is under a patent.²⁵ The originality of this ECR thruster lies in its coaxial geometry that allows a reduction in its diameter compared to typical wave-guide ECR sources, and in the low power consumption (around 50 W). This coaxial thruster geometry is similar to that used in some other microwave thrusters, such as in Refs. 26 and 27, except that it uses a diverging magnetic field to operate near the ECR condition and to enhance the plasma expansion, and it operates at lower flow rates and high powers. An experimental characterization of ECR plasma thruster has been led in the past few years using argon and xenon as propellant gases. In the previous work with xenon,^{28,29} a mass utilization efficiency of 50% and an ion energy of 350 eV were measured. It was shown that Xe^+ ion energy strongly depends on the pressure inside the source. The effect of the magnetic field topology and the position of the resonance zone in the ECR source have also been investigated. A significant improvement of the thruster performance has been achieved by widening the resonance region and reducing the distance between this region and the back of the cavity.³⁰

In this paper, the effect of the ECR source cavity geometry on the thruster performance is assessed. In parallel, an analytical thruster discharge model³¹ developed originally for HPTs is adapted to the ECR plasma thruster and the results are compared to the experimental measurements.

The principle of the ECR plasma thruster and the analytical discharge model are presented in Sec. II. The experimental facilities and diagnostics are introduced in Sec. III. Section IV presents the experimental results and the comparison with the analytical model. Finally, Sec. V summarizes the results and gives concluding remarks on the thruster operability.

II. PRINCIPLE AND MODEL OF ECR PLASMA THRUSTER

A. General principle of ECR plasma thruster

The operating principle of the thruster is based on the absorption of microwave power by electron cyclotron resonance. The resonant absorption occurs when the frequency of the microwave electric field ω_{rf} coincides with the cyclotron frequency ω_{ce} of electrons in the presence of an externally applied magnetic field. At this condition ($\omega_{rf} = \omega_{ce}$), the electrons see a stationary electric field, and are continually heated by the right-hand polarized component of the electromagnetic wave. Thus microwave energy is absorbed collisionlessly. In the presence of complicated source geometries and magnetic field topologies, as well as non-uniform plasmas, the microwave propagation and absorption process is very complex, and the ECR phenomenon is still an active area of research.¹³ A plasma is created inside the thruster by injecting and ionizing a neutral gas, and with sufficient input power, a high density plasma can be produced. A diverging magnetic field is applied using either a set of permanent magnets, or a coil, and plasma expansion in the resulting magnetic nozzle occurs outside the thruster. This leads to an ambipolar electric field that directly accelerates ions to high velocities, similarly to HPTs,^{11,12} and sufficient electrons with high energy escape the potential barrier to ensure a quasi-neutral and a current-free plasma exhaust. Neutrality of the beam is naturally enforced in the thruster by using floating walls so that no net dc current can be extracted. Thus a hollow cathode neutralizer is not needed. Eventually, the plasma detaches from the magnetic nozzle downstream ensuring that a net thrust force can be produced.

B. Analytical thruster discharge model

To describe and model the general behavior of the ECR thruster, we modify a recent analytical discharge model developed for HPTs. The detailed model formulation can be found in Ref. 31, and we present only a brief overview here. The model considers two separate regions of the thruster: the plasma source region (i.e., the inside of the thruster), and the downstream plasma expansion in the diverging magnetic field. In both regions, the plasma is quasi-neutral, and the electrons are assumed isothermal.

In the plasma source, a uniform magnetic field is present that helps to radially confine the plasma, as well as to allow ECR to occur. Because of radial plasma losses, as well as ionization, both the plasma density and the neutral gas density have an axial variation along the length of the thruster. This variation is accounted for by solving the relevant continuity, momentum, and energy conservation equations in 1D.

A self-similar radial plasma density profile is used to more realistically describe the plasma, while a semi-empirical approach is used to account for anomalous cross-field diffusion usually seen experimentally.³¹ In this way, the 1D conservation equations effectively represent cross-section averaged equations, and so are quasi 2D. The radial neutral gas profile is assumed to be uniform, but the axial variation is self-consistently accounted for.

In the downstream region, ionization is ignored, and the plasma is assumed to expand along an axially varying cross-section that changes so as to conserve magnetic flux. At some point, downstream the ion gyroradius becomes equal to the radius of the plasma cross-section and the ions are assumed to demagnetize and plasma detachment occurs. Experimental measurements,^{32,33} as well as recent detailed numerical simulations,^{34,35} have shown that plasma detachment can occur by ion demagnetization, even if electrons are still magnetized.

For a given thruster geometry and operating conditions (i.e., mass flow rate and input power), the model can be solved and relevant plasma (such as the electron temperature) and thruster parameters (such as the thrust) determined. Similar to Ref. 31, no explicit model for the microwave/plasma coupling is developed, and only the power absorbed by the plasma (which can be directly measured in the experiment) can be found. The above model has been modified to account for the coaxial thruster geometry used here, which introduces an additional plasma loss surface, and a modified radial density profile. These modifications, together with the relevant model equations, are discussed in the Appendix. Because of the small antenna diameter compared with the thruster source diameter (see Sec. III below), the difference in the model results for the coaxial system used here, and a cylindrical system, is typically only a few percent.

III. EXPERIMENTAL APPARATUS AND METHODS

A schematic of the ECR plasma thruster is shown in Fig. 1. The thruster consists of two coaxial cylinders connected to a microwave (MW) coaxial transmission line. A backwall made of dielectric (Macor, $\epsilon_r \approx 6$) is used to protect the MW line from direct contact with the plasma. Argon

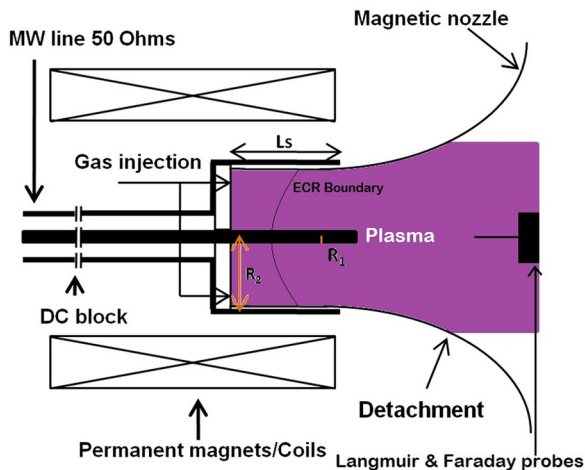


FIG. 1. Schematic of the ECR plasma thruster and probes, figure is not to scale.

or xenon propellant gas is injected into the thruster through a number of small holes in the backwall. The power absorbed by the plasma is measured with a bi-directional coupler placed in the MW transmission line just before the thruster. The typical power coupling efficiency of the plasma source with the MW transmission line is between 70% and 95%, depending on the propellant gas flow rate, geometry, plasma density, and the size and location of ECR region. An external magnetic field is produced using either a set of permanent magnets (see Ref. 29), or a multi-layer, water-cooled coil having a length of 55 mm, and an average diameter of 61.5 mm. The magnetic field produced by the coil has been simulated numerically using COMSOL, and verified experimentally by taking measurements with a GM05 Hirst Gaussmeter, as shown in Fig. 2 for a coil current of 130 A.

The experimental characterization of the ECR plasma thruster is performed for two different configurations. The first configuration has an outer coaxial cylinder diameter, $2R_2$, of 13 mm and the magnetic field is produced using permanent magnets, while the second configuration has an outer diameter of 27 mm and the magnetic field is produced with the coil. The backwall and exit of the thruster are located at axial positions of 20 mm and 35 mm, respectively, from the coil center (see Fig. 2). For both configurations, the length of the thruster cavity, L_s is 15 mm ($35\text{ mm} - 20\text{ mm} = 15\text{ mm}$), and the diameter of the MW antenna, $2R_1$, is 1.85 mm. With

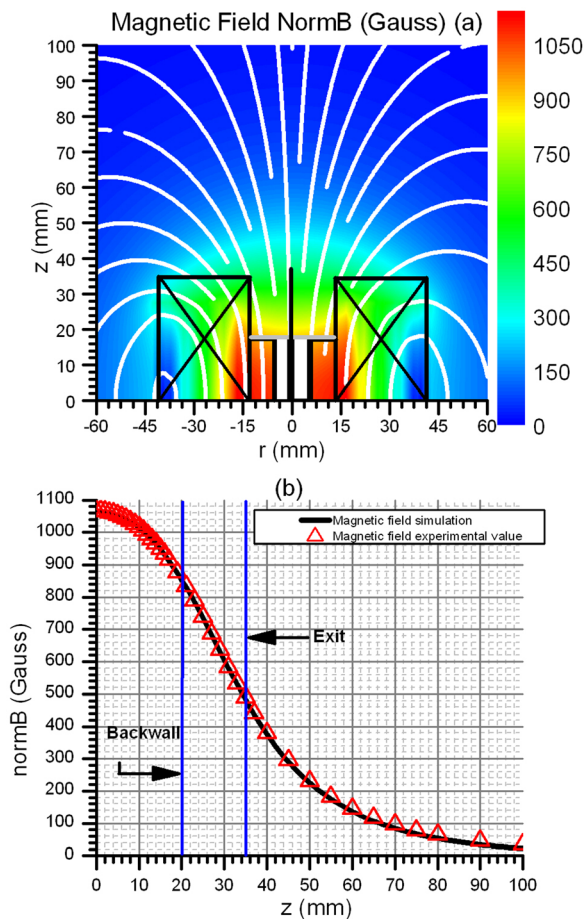


FIG. 2. Magnetic field produced by the coil at 130 A. Simple mirror configuration, comparison between simulation, and experimental values measured on axis.

the coil current at 130 A, the difference between the magnetic field from the permanent magnet and the coil is small inside the plasma source. Both the outer cylinder and the MW antenna are floating due to the presence of a DC-block located between the bi-directional coupler and the thruster (see Fig. 1). This DC-block ensures that no net DC current is extracted to the walls of the thruster, and hence that the thruster is current-free similar to a HPT.^{11,12} Power is supplied to the MW transmission line via a combination of a Kuhne Electronic signal generator, and a linear power amplifier. The MW frequency is nominally tuned to 2.45 GHz, and the output power is adjustable from 0 to 100 W. A circulator with a 50 Ohm load is used to protect the MW amplified from any reflected power.

The ECR plasma thruster is characterized in the B61 facility at the Onera research center in Palaiseau, France. The B61 is a cylindrical vacuum chamber 4 m long and 1 m in diameter, and is equipped with a turbomolecular pump (Pfeiffer TPU 2200 l/s) and a cryo-pump (CTI-cryogenics Helix technologies), which give a base pressure below 10^{-6} mbar and a measured total pumping speed of 8000 l/s with xenon. When the thruster is operating, the measured vacuum chamber pressure is sufficiently low that neutral gas ingestion²¹ by the thruster is estimated to increase the effective mass flow rate by only about 1%–2%. Depending on the mass flow rate, the effective pressure inside the plasma source for configuration 1 is estimated to be between $4.0\text{--}8.0 \times 10^{-3}$ mbar for argon and $1.4\text{--}4.2 \times 10^{-3}$ mbar for xenon, while for configuration 2 it is estimated to be between $0.3\text{--}1.3 \times 10^{-3}$ mbar. In order to ignite the plasma in the thruster, it is necessary to make use of a high flow rate gas puff (above 4 SCCM), together with a high MW power (about 50 W). Once the plasma has been ignited, the flow rate and power can then be reduced.

Four electrostatic probes are used for the characterization of the thruster plume: a gridded Faraday probe for ion current density measurements, a retarding potential analyzer (RPA) and a Hidden PSM ion analyzer for ion energy distribution function measurements, and a Langmuir probe (LP) to measure the electron temperature. The three custom built probes (Faraday, RPA and LP) are mounted onto a motorized rotation stage in order to perform angular scans (between $\pm 90^\circ$, where 0° is on the thruster central axis) of the plume. The Hidden PSM ion analyzer is mounted at the far end of the vacuum chamber. The Faraday probe and the RPA are placed about 30 cm away from the thruster exit so as to minimize any perturbation during operation of the thruster.

The Faraday probe consists of a collector plate that is biased at -200 V to repel high energy electrons. This potential is deduced from measured I-V characteristics taken with the probe to obtain the ion saturation current. A floating grid is placed in front of the collector plate in order to screen the plasma from the applied bias voltage, and minimize the effect of sheath expansion (which can artificially increase the collecting area of the probe, and hence the measured current). The collected ion current is measured with a Keithley picoammeter. The ion current density is then obtained by dividing the measured current by the area of the collection aperture (which is 6 mm in diameter), taking into consideration the grid transparency (which is about 50%).

The RPA consists of an outer floating metallic grid, three biased grids, and a collector plate. The first and third grids repel electrons, while the second grid is the ion energy analysis grid whose potential is scanned in order to filter the incoming ions as a function of their kinetic energy. Similar ion energy distributions were obtained with the RPA and the Hidden PSM ion analyzer.

Because of the small size of the thruster, as well as the presence of the MW antenna, it is not possible to measure the electron temperature (and hence plasma density) directly inside the thruster. Thus the Langmuir probe is located about 8 cm from the thruster exit. Both axial measurements (over a distance of about 10 cm) and angular measurements showed that the electron temperature was spatially uniform in this region. The probe is similar to that described in Ref. 36 and consists of two small 0.125 mm diameter tungsten wires embedded in a small ceramic tube. One of the probe tips serves as a reference electrode to allow the measurement tip to follow any oscillations in the plasma potential. Both wires are placed perpendicular to the magnetic field lines, and the tip diameters are smaller than the electron gyroradius. The electron temperature is found by taking moments of the electron energy probability function (EETF), which is determined from the second derivative of the measured I-V curve.³⁷

By taking measurements of the ion beam current density, J_i , with the Faraday probe at different angular positions, it is possible to obtain an angular profile of the current density which can then be integrated to calculate the total ion beam current, I_i . Assuming that the ion beam plume is axis-symmetric, and that negligible ionization occurs after the probe location, the total ion beam current follows simply from the integral of the current density over the surface swept by the Faraday probe

$$I_i = \int_{-\pi/2}^{\pi/2} J_i(\theta) \pi D^2 \sin(\theta) d\theta. \quad (1)$$

Here, D is the distance of the Faraday probe to the thruster exit and θ is the angle of the probe with respect to the thruster central axis at $\theta = 0$.

The mass utilization efficiency $\eta_m = \frac{I_i m_i}{\dot{m}_g q} = \frac{\dot{m}_i}{\dot{m}_g}$ is the ratio of the ion mass flow rate \dot{m}_i over the total input gas mass flow rate \dot{m}_g . It is calculated from the total ion beam current found from Eq. (1), and represents the fraction of propellant gas that is effectively ionized and used to generate thrust. The ion energy E_i is obtained from measurements using either the RPA or the Hidden ion analyzer. The effective thrust F_p can be found from the angular profile of the ion current density and the ion velocity using Eq. (2).

$$F_p = \int_{-\pi/2}^{\pi/2} J_i(\theta) \frac{m_i}{q} v_i \pi D^2 \sin(\theta) \cos(\theta) d\theta, \quad (2)$$

where v_i is the mean ion velocity (on the axis) deduced from the kinetic energy E_i . It should be noted that angular measurements of the ion energy were taken and that no significant variation of ion energy was observed,²⁸ thus we use a single value for the ion velocity (usually measured at the centerline for all the presented data). Equation (2) above is similar in

form to that used in Ref. 21, except that there the current density is known along a radial profile, whereas here the current density is known along an angular profile. This equation effectively represents the net axial ion momentum that flows across the angular surface used for the probe measurements.

The divergence factor efficiency $\eta_D = \frac{F_p}{\dot{m}_i v_i}$ is the ratio between the effective thrust calculated with the measured angular current density distributions, and the ideal distribution on axis.²¹ The power efficiency $\eta_e = \frac{I_i E_i}{P_{MW}}$ compares the ion kinetic power in the plasma jet with the absorbed MW power. The estimated total thruster efficiency is calculated with the usual formula $\eta_T = \eta_m \eta_e \eta_D^2 = \frac{F_p^2}{2\dot{m}_g P_{MW}}$. Finally, the specific impulse is calculated from $I_{sp} = \frac{F_p}{\dot{m}_g g_0} = \frac{\eta_D \eta_m v_i}{g_0}$, where g_0 is the standard gravitational acceleration constant (9.81 m/s²). Here, it can be seen that the specific impulse depends directly on the level of propellant mass utilization.

IV. RESULTS

A. Configuration 1

The data in this section relate to the 13 mm diameter thruster. The present set of results is obtained for different mass flow rates with two different propellant gases: argon

and xenon. The experimental results for the first configuration are shown in Fig. 3. The maximum current density is on the thruster central axis, and it can be seen that the current density tends to increase with propellant mass flow rate. In particular, the current density on the axis, and the total ion beam current, increases by a factor of 2 when the flow rate is increased from 0.1 mg/s to 0.2 mg/s. However, with xenon, no change in ion current density is seen on the thruster axis when the flow rate is increased from 0.2 and 0.3 mg/s, although the total ion beam current is larger (see Table I). This phenomenon was not seen in argon (not shown in Fig. 3), probably due to the lower ionization degree compared with xenon. The increase is only seen in the “wings” of the angular profile, which implies that the plume is more divergent. The normalized ion energy distribution indicates a maximum value of about 280 eV at the lowest mass flow rate (0.1 mg/s) with an absorbed power of 40 W for Xenon. For both gases, the ion energy increases when the mass flow rate is reduced. In some of the ion distributions in Fig. 3 (and also in the distributions discussed in Sec. IV D below), a second smaller peak can be seen at low energies. This peak tends to get less significant as the flow rate decreases, which is consistent with the presence of ion-neutral collisions. Because of the small size of this second peak compared with the main peak, the effect of downstream

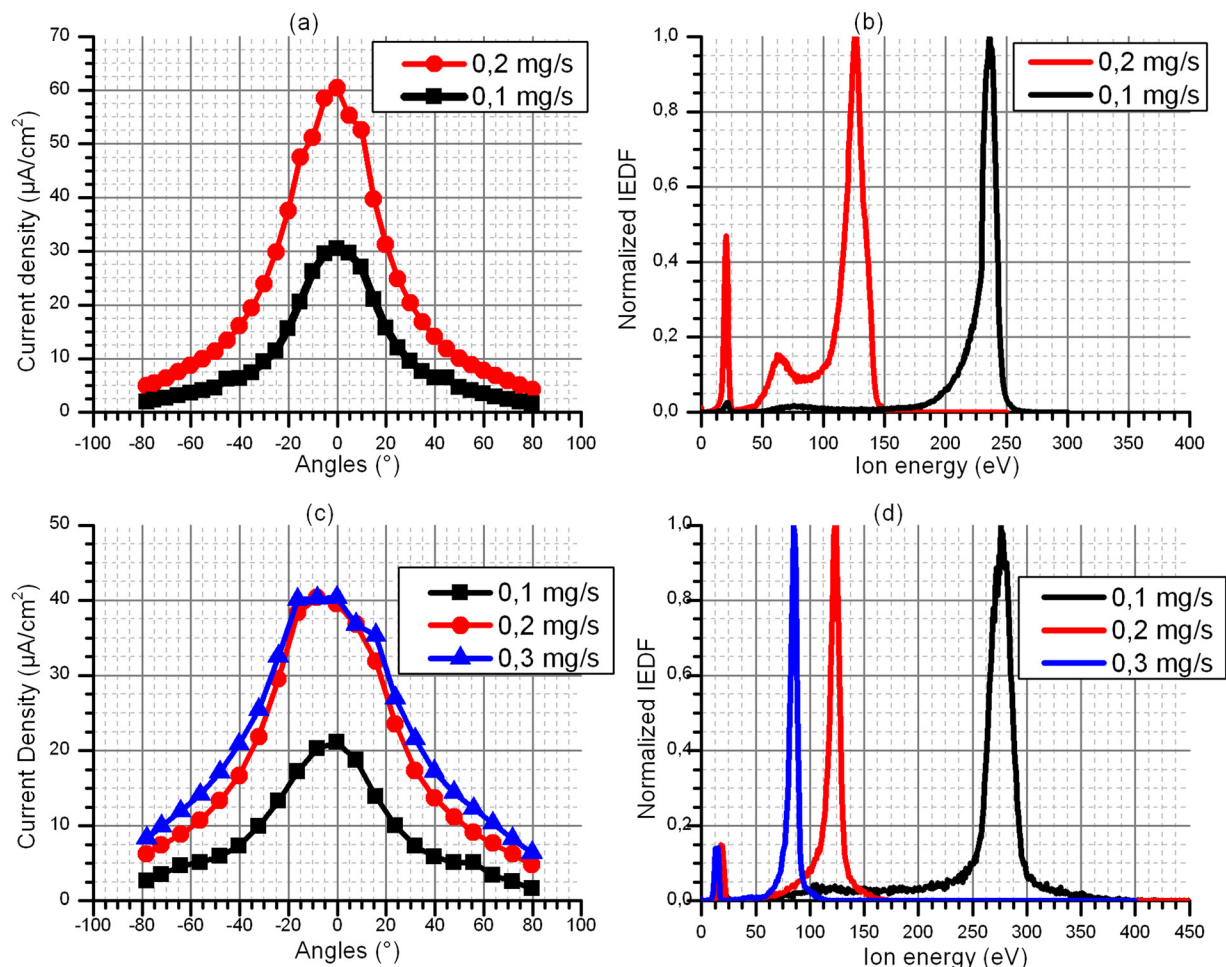


FIG. 3. Angular profile of the ion current density (Faraday Probe) and the ion energy distribution function measured (from the Hidden ion analyzer) in configuration 1 with (13 mm outer diameter). (a) and (b) using argon at 35 W (c) and (d) using xenon at 40 W.

TABLE I. Summary of ECR plasma thruster performance in configuration 1 (13 mm outer diameter).

Gas	Argon	Argon	Xenon	Xenon	Xenon
Mass flow rate (mg/s)	0.1	0.2	0.1	0.2	0.3
Power absorbed (W)	35.7	37.3	40.4	40.7	40.7
Ion energy (eV)	235	125	280	125	90
Ion current (mA)	30	67	30	65	80
Thrust (mN)	0.31	0.5	0.58	0.84	0.85
Isp (s)	315	257	590	428	289
Mass utilization efficiency (%)	12	14	41	44	36
Power efficiency (%)	20	22	21	20	18
Divergence efficiency (%)	74	73	70	70	68
Thruster efficiency (%)	1.3	1.7	4.2	4.3	3

ionization and ion-neutral collisions is not expected to be significant. Indeed, during thruster operation the vacuum chamber pressure is measured to be between about 6×10^{-6} mbar and 2×10^{-5} mbar (depending on the flow rate), which gives an ion mean free path of the order of several meters.

In Fig. 4, the electron temperature is shown as a function of the mass flow rate for both argon and xenon. Below about 0.1 mg/s, the mass flow rate has a strong influence on the electron temperature, and values above 15 eV are measured at the lowest flow rate. Because the neutral gas density inside the thruster decreases with mass flow rate, the discharge ionization/loss balance can only be maintained if the electron temperature becomes very high. A secondary consequence of this high electron temperature is that a larger ambipolar electric field is produced, leading to strong ion acceleration in the downstream region (Fig. 3).

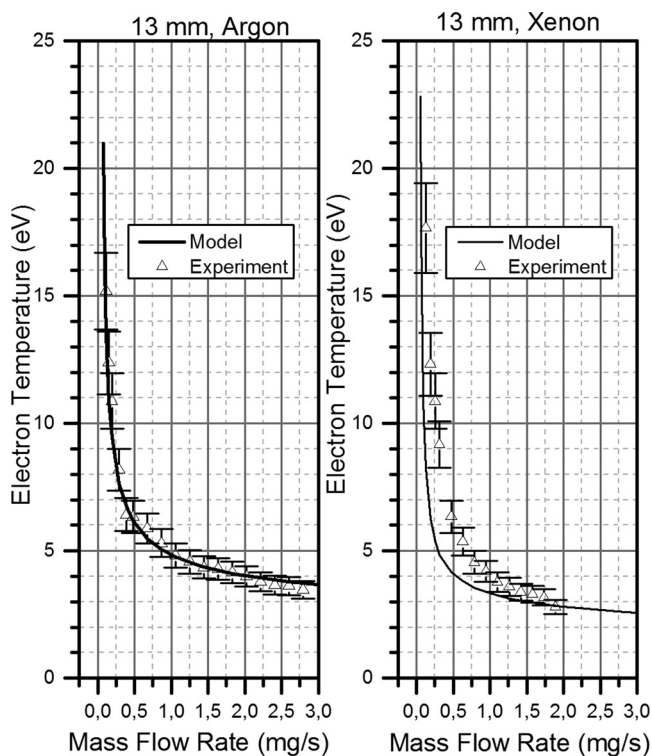


FIG. 4. Electron temperature 8 cm from the thruster exit in configuration 1 (13 mm outer diameter). Symbols: measurements with the Langmuir probe. Line: analytical discharge model. The absorbed power is 20 W.

The performance of the ECR thruster in configuration 1 is presented in Table I. For similar absorbed powers, the maximum mass utilization efficiency is better with xenon (45%) than argon (14%), while the plume divergence efficiency is around 70%, and more efficient at lower mass flow rates (particularly for argon). The maximum produced thrust of 0.85 mN is obtained at xenon flow rates of 0.2 mg/s and 0.3 mg/s (with the same microwave power of 40 W). The lower ion current at 0.2 mg/s is compensated for by the higher ion energy at this flow rate. A maximum thruster efficiency of about 4.3% is obtained for configuration 1, which is estimated using the known flow rate (0.2 mg/s) of xenon and 40 W of absorbed microwave power. The low values of specific impulse for argon compared with xenon are due to the poor mass utilization efficiency in argon. If the mass utilization increases, the specific impulse will be larger because of the higher effective ion velocity.

It should be noted that the electron temperatures in Fig. 4 were measured at a lower MW power than the ion energies in Fig. 3 and in Table I. As the MW power level increases, neutral depletion occurs inside the thruster, and as a result the effective pressure decreases. As seen in Fig. 4 though, the electron temperature is very sensitive to the effective flow rate under the conditions used in the experiment. Due to limitations of the electronics used to bias the Langmuir probe it was not possible to measure temperatures above about 20 eV. Hence, lower powers were chosen for the results in Fig. 4. Better thruster performance and higher ion energies were however obtained at higher powers, which were chosen for the results in Fig. 3 and Table I. At similar power levels (not shown), the ratio of ion energy to electron temperature was about 5, indicating that sufficient electrons can escape the thruster to neutralize the ion beam.^{9,21}

Based on the total ion beam currents measured (and shown in Table I), we can infer an average current density by dividing by the thruster cross-sectional area. This gives values of between about 20–60 mA/cm² for xenon. Measurements of the total beam current are not readily available for other expanding plasma thruster such as Helicon thrusters, because in these systems the direct thrust is usually measured as opposed to the ion current and mass utilization. However, Ref. 38 gives values of about 10 mA/cm², while Ref. 21 gives values of about 5 mA/cm² for gridded ion thrusters, and about 100 mA/cm² for Hall thrusters.

B. Comparison with analytical discharge model

The analytical calculation of the electron temperature T_e from the discharge model is compared with the Langmuir probe measurements in Fig. 4. The analytical model is in very good agreement with the experimental results for argon over the entire range of mass flow rates tested, while for xenon the electron temperature obtained with the model is slightly lower. The trend, particularly at lower mass flow rates below 1 mg/s, is however similar. Because of the semi-empirical radial plasma confinement approach used in the model (see the Appendix), there is some uncertainty in the model results (which is expressed as the blue shaded envelope in Fig. 5; see below). This uncertainty though (just a

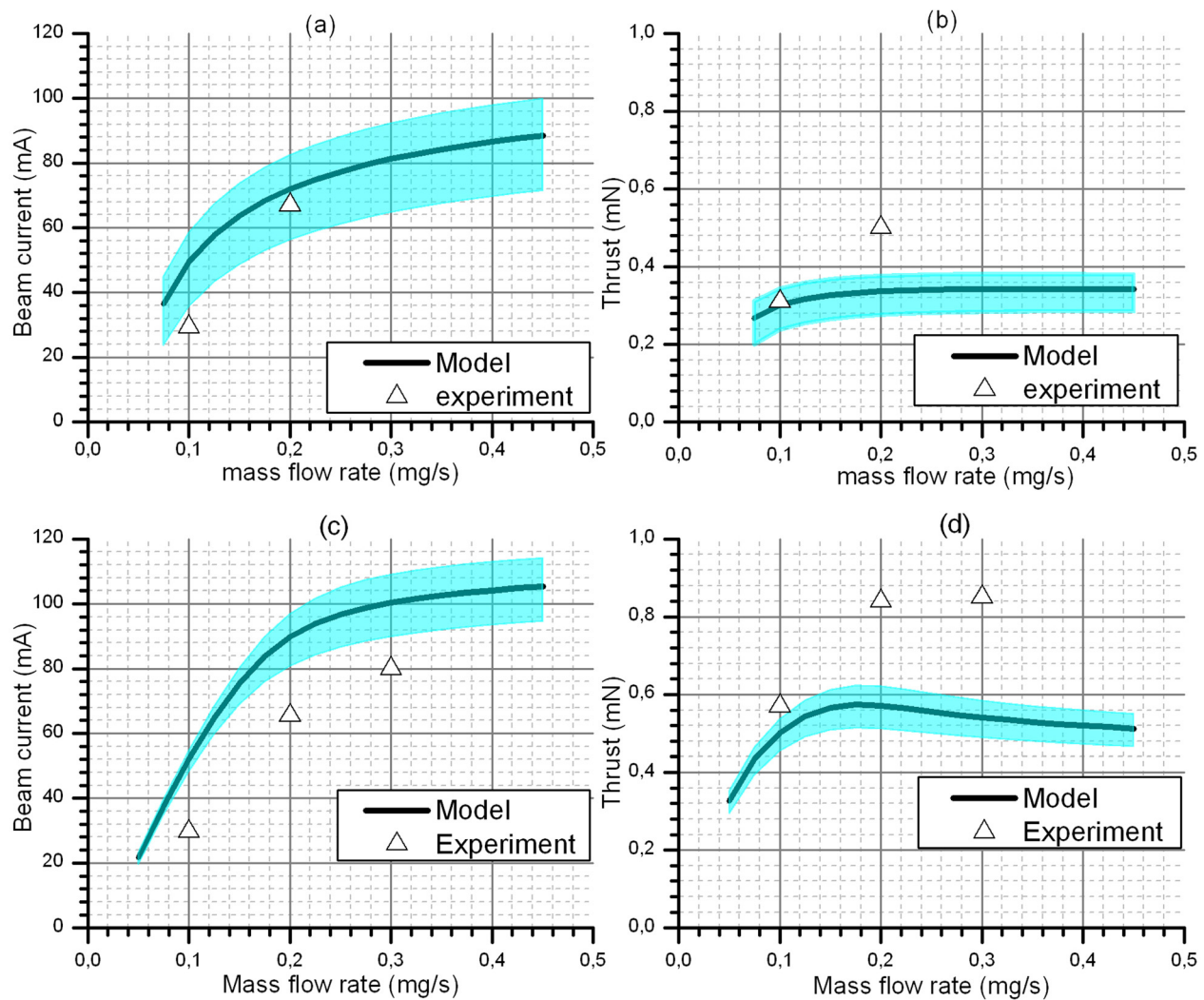


FIG. 5. Thruster performance in configuration 1 (13 mm outer diameter) from experimental measurement and analytical discharge model. (a) and (b) using argon; (c) and (d) using xenon. The shaded region is due to the heuristic formulation of plasma confinement in the model.

few percent and not shown in Fig. 4) is too small to explain the difference with the xenon experimental results. The measured EEPFs (not shown) are in general non-Maxwellian. However, the change to the ionization rate factor compared to a Maxwellian distribution (which is assumed in the model) with a similar effective temperature was calculated to be typically no more than about 10%–15%. Consequently, the difference between the model and experimental results may be due to neutral gas heating, which would change both the radial neutral gas profiles,³⁹ and reduce the neutral gas density inside the thruster because of the faster moving neutrals.

In Fig. 5, the total ion beam current and the thrust estimated from the experimental measurements are compared with the results of the analytical model. The total ion beam current from the model is in very good agreement with the measurements of the Faraday probe with argon. In the case of xenon, the ion beam current results are close to the experimental values, and the variation with the mass flow rate is similar. The thrust calculated with the model and estimated from experimental measurements agrees well at low flow rates, but diverges by a few tens of percent at higher flow

rates. In the model we have treated the plasma expansion in the magnetic field using a simple 1D model that assumes a radially uniform axial magnetic field, and have used a simple criterion for plasma detachment. Comparison of a similar model with a more accurate 2D model⁴⁰ has shown that the thrust force is typically underestimated by about 20%–30%. In addition, as seen in Fig. 4, the model electron temperatures for xenon are also underestimated, and as shown in the Appendix, the thrust force is directly proportional to the electron temperature. Nevertheless, the model results are in reasonable agreement, and capture most of the parameter scalings.

C. Optimization of the thruster using the model

The analytical discharge model agrees with the electron temperature and total ion beam current measurements, so it is reasonable to use the model in order to optimize the performance of the thruster. The model shows that the principle performance losses of the thruster are due to plasma losses on both the radial walls and the backwall. As previously discussed in Ref. 31, improved performance is expected with a

larger magnetic field, which improves both the plasma confinement, and increases the thrust component from the magnetic nozzle. In the present system, the magnetic field strength cannot be increased significantly, because of the need to maintain the ECR condition. Consequently, only the geometry of the coaxial thruster source (length and diameter) can be optimized. The model predicts that the thruster efficiency can be more than doubled by doubling the thruster diameter, as demonstrated in Fig. 6 for thrusters with diameters of 13 mm and 27 mm, respectively, for 0.2 mg/s. This occurs because as the diameter increases, a larger ratio of ions is extracted from the thruster than is lost to the walls. Consequently, more ions are usefully used to generate thrust, and lower relative power losses are predicted. With the present experimental setup, doubling the outer diameter of coaxial thruster cylinder is relatively simple due to its initial design.

D. Configuration 2

Figure 7 shows the experimental data from the measurement with the new thruster (configuration 2) having a larger outer diameter of 27 mm. The experiments are performed with xenon gas only because of the better thruster efficiency obtained both in Sec. IV A, and predicted by the model (not shown). The absorbed power is kept constant at 30 W for all measurements. Compared to the performance of configuration 1, the ion current density on-axis is higher for the same mass flow rate, and with a lower power. The same evolution of the angular profile of the ion current density is observed when the mass flow rate is increased from 0.2 mg/s to 0.4 mg/s. This effect could be induced by increased charge exchange and collisional phenomenon due to the higher pressure in the plume. The ion energy is of the same order as that in configuration 1 despite the slightly lower power deposited in the plasma. Figure 8 shows a comparison between electron temperature from the Langmuir probe and the analytical discharge model. Again, the model reproduces the same

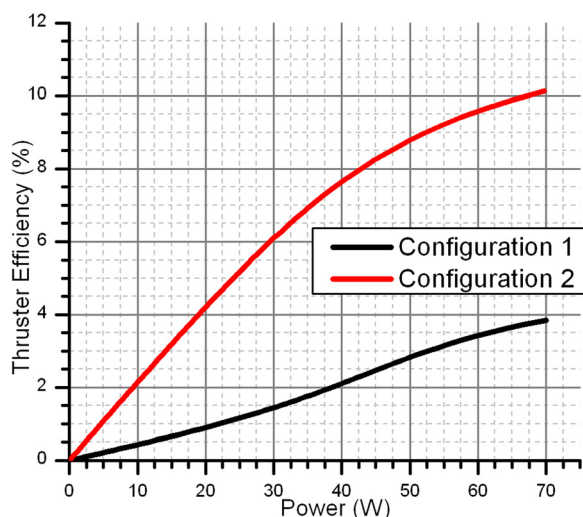


FIG. 6. Analytical calculation of thruster efficiency as a function of absorbed power for the two outer diameter configurations with a mass flow rate of 0.2 mg/s.

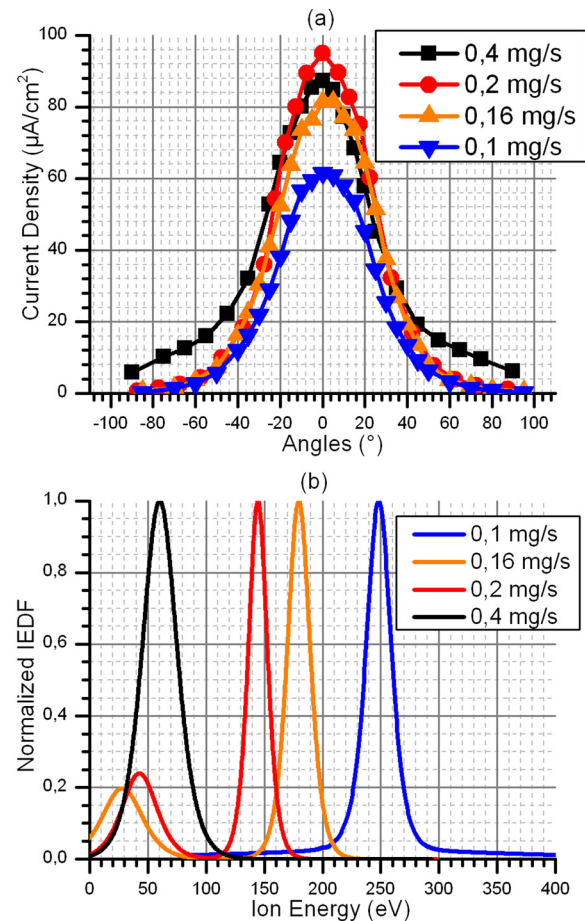


FIG. 7. Angular profile of the ion current density (Faraday probe) and the ion energy distribution function (from the RPA probe) measurements in configuration 2 (27 mm outer diameter), for 30 W of absorbed power.

behavior and scaling. At the same power, the electron temperatures are higher in configuration 2 than configuration 1, which is favorable for the thrust (see Eq. (A8) in the Appendix). These higher electron temperatures occur because at the same mass flow rate, the effective pressure (and hence neutral density) inside the thruster is lower due to the larger cross-sectional area of configuration 2 compared with configuration 1. Table II summarizes the ECR thruster performance for the configuration 2. The calculation of the total ion current confirms the better production and extraction of the new source, and at 0.1 mg/s we obtain a mass utilization efficiency of 62%. The effective thrust indicates a higher divergence efficiency of 83%, in the range 0.1–0.2 mg/s. The maximum thruster efficiency for configuration 2 is 16%, which has been estimated using the known xenon flow rate of 0.1 mg/s and 30 W of absorbed microwave power, and which also gives a thrust of about 1 mN. The thruster efficiency is improved when reducing the mass flow rate, in particular because of the higher final ion energy, higher divergence efficiency, and the improved mass utilization efficiency. Figure 9 presents a comparison of the experimental and model results for configuration 2. The ion beam current predicted by the analytical model is close to the experimental results, and the trend with mass flow rate is well reproduced. However, the thrust is again underestimated

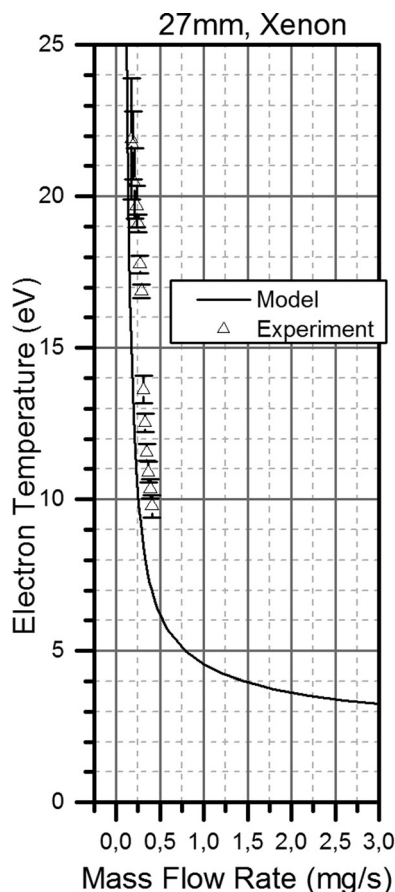


FIG. 8. Electron temperature in configuration 2 (27mm outer diameter). Symbols: measurements with the Langmuir probe. Line: analytical discharge model. The absorbed power is 20 W.

by a few tens of percent in the model, probably for the same reasons as those discussed in Sec. IV A for configuration 1.

V. CONCLUSION

In this paper, a compact cathodeless ECR plasma thruster has been presented and a detailed experimental characterization of the plasma source, as well as a comparison with an analytical discharge model, has been performed. Agreement of the model with the experimental measurements, together with a subsequent analytical study, identified

TABLE II. Summary of ECR thruster performance in configuration 2 (27 mm outer diameter).

Gas	Xenon	Xenon	Xenon	Xenon
Mass flow rate (mg/s)	0.1	0.16	0.2	0.4
Power absorbed (W)	30.0	30.0	30.0	30.0
Ion energy (eV)	250	150	100	50
Ion current (mA)	45	62	71	101
Thrust (mN)	0.98	1.04	0.97	0.825
Isp (s)	993	662	495	210
Mass utilization efficiency (%)	61	53	48	34
Power efficiency (%)	38	31	24	16
Divergence efficiency (%)	83	83	83	70
Thruster efficiency (%)	16	11	8	3

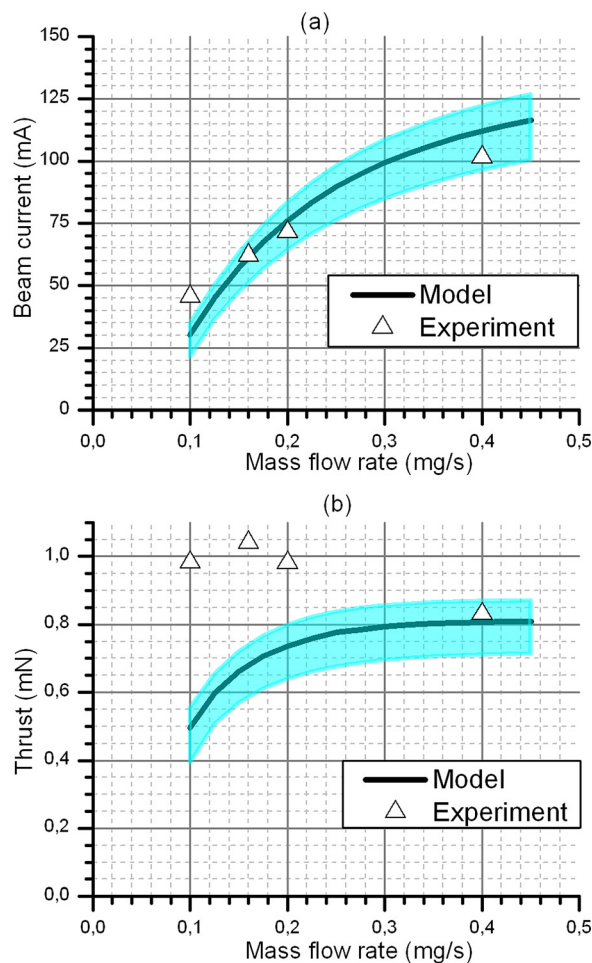


FIG. 9. Thruster performance in configuration 2 (27 mm outer diameter) from experimental measurements and the analytical discharge model using xenon. The shaded region is due to the heuristic formulation of plasma confinement in the model.

the thruster diameter as a possible performance optimization parameter. A new thruster was constructed and tested, and a higher ion beam current was experimentally demonstrated. In order to directly validate the operation of a new thruster however, it is usually necessary to perform direct thrust measurements with a sensitive force balance. From these thrust measurements, the relevant efficiencies can then be determined. In this work, we have estimated the performance based on measurements of the total ion beam current and ion energy obtained from angular measurements of the plasma plume downstream of the thruster. Because of the large pumping speed of the vacuum chamber used (due in large part to the presence of a cryo-pump) the downstream chamber pressure is very low even when the thruster is operating, and estimates of gas ingestion were estimated to have a minimal effect. Thus, the estimated performance from the electrostatic probe measurements is expected to be representative of the true thruster behavior. Based on these measurements, the best thruster performance was found to give a thrust of 1 mN, a thruster efficiency of 16%, and a specific impulse of almost 1000 s in xenon. Future works on the ECR plasma thruster will include direct thrust measurements on a thrust balance.

The improvement obtained demonstrates the importance of the plasma source geometry on magnetic-nozzle plasma thruster performance, and in particular, highlights the need to reduce plasma losses on the radial and backwall compared with the open end of the thruster. The predictions of the analytical model are in reasonable agreement with a wide range of experimental measurements, and it serves as a useful tool for initial thruster designs and efficiency estimates without requiring expensive computational time and resources. The detailed physics of the ion acceleration and detachment process are however still not well understood, and improved model predictions will benefit from further experimental and theoretical work.

ACKNOWLEDGMENTS

The authors would like to thank A. Aanesland for the Langmuir probe electronic system. T.L. acknowledges financial state aid managed by the Agence Nationale de la Recherche as part of the program “blanc” under the Reference No. ANR-2011-BS09-40 (EPIC), and the program “Investissements d’avenir” under the Reference No. ANR-11-IDEX-0004-02 (Plas@Par).

APPENDIX: ANALYTICAL THRUSTER MODEL

The axial ion continuity equation (Eq. (5) in Ref. 31) can be modified by adding an additional loss term on the right-hand side to account for radial plasma losses on the antenna. Thus, the continuity equation becomes

$$\frac{d}{dz}(\beta n v_z A_0) = K_{iz} \beta n n_g A_0 - 2\pi R_{eff} h_R u_B. \quad (\text{A1})$$

Here, n is the plasma density, n_g is the neutral gas density, $K_{iz} = K_{iz}(Te)$ is the ionization rate factor, A_0 is the cross-sectional area of the thruster, v_z is the axial ion velocity, $u_B = \sqrt{\frac{qT_e}{m_i}}$ is the Bohm velocity with q being the elementary charge, Te being the electron temperature, and m_i being the ion mass, h_R is the sheath edge-to-center plasma density ratio, and β is a factor accounting for the radial plasma density profile (see below). The additional loss surface due to the antenna allows the definition of an effective thruster radius given by $R_{eff} = R_2 + R_1$. With this definition, Eq. (A1) has an identical form to that in Ref. 30, and consequently, the equations are appropriately modified. The axial neutral gas density, n_g , is self-consistently solved by considering the mass conservation equation for neutrals and ions

$$\dot{m}_g = M n_g v_g A_0 + M n v_z A_0,$$

where \dot{m}_g is the input mass flow rate to the thruster and M is the elementary mass of particle gas. This equation can then be combined with Eq. (A1). Depending on the thruster operating conditions, the axial neutral density variation can be significant. The value for h_R in Eq. (A1) is obtained using the same semi-empirical method as that used in Ref. 31 and is given by

$$h_R \approx \frac{0.4}{\sqrt{1 + c(R_2/r_{ci})^2}}, \quad (\text{A2})$$

where r_{ci} is the ion gyroradius, and $c = 0.68$. The value for β is obtained by finding the radially averaged plasma density. In Ref. 31, this was calculated using a semi-empirical function for the radial density profile that was shown to be in good agreement with experimental measurements. In the present coaxial thruster, there is no available information on the radial profile, and so as a zero order estimate we use the same normalized function as in Ref. 31, but assume that the density is zero for radii less than the antenna radius. Thus, the radially averaged density becomes

$$\beta = \left(\frac{1}{7d}\right) \frac{R_2^2}{(R_1^2 - R_2^2)} \left((1-d)^7 - (1-d) \left(\frac{R_1}{R_2}\right)^2 \right)^7, \quad (\text{A3})$$

where $d = (1 - h_r^{\frac{1}{6}})$.

By combining the continuity and momentum equations, the electron temperature is found numerically from Eq. (A4) below

$$\begin{aligned} -2 - \xi \ln\left(\frac{1-\xi}{1+\xi}\right) + 2\sqrt{1-\xi^2} \left[\arctan\left(\frac{1-\xi}{\sqrt{1-\xi^2}}\right) \right. \\ \left. - \arctan\left(\frac{-1-\xi}{\sqrt{1-\xi^2}}\right) \right] = \gamma, \end{aligned} \quad (\text{A4})$$

where

$$\begin{aligned} \gamma &= a \frac{K_{iz}}{u_B} - b, \\ \xi &= \frac{\eta_d}{1 - \frac{u_B b}{K_{iz} a}}, \\ a &= \frac{\Gamma_0 L_s}{v_g}, \\ b &= \frac{2h_r L_s}{\beta R_{eff}}, \\ \Gamma_0 &= \frac{\dot{m}}{A_0 m_i}. \end{aligned}$$

Here, v_g is the neutral gas velocity (assumed constant), \dot{m} is the input neutral mass flow rate, and η_d is the propellant utilization. Once the electron temperature is known, the maximum plasma density, n_0 , in the thruster is found from

$$\eta_d = \frac{\beta n_0 u_B}{2\Gamma_0}. \quad (\text{A5})$$

The Mach number, $M_{det} = \frac{v}{u_B}$, at which the ions detach from the magnetic field in the downstream region is then obtained by numerically solving the equation

$$\frac{1}{2}(M_{det}^2 - 1) - \ln(M_{det}) = \ln\left(\frac{qB_0^2 R_s^2}{m_i T_i}\right), \quad (\text{A6})$$

where B_0 is the magnetic field strength at the thruster exit, and T_i is the ion temperature (assumed constant at 0.2 eV). The total power absorbed by the plasma is determined from

$$P_{abs} = \frac{1}{2}q\beta n_0 u_B A_0 (\varepsilon_c + \varepsilon_{ic} + \varepsilon_{ec}) + \frac{1}{2}q\beta n_0 u_B A_0 (\varepsilon_c + \varepsilon_{io} + \varepsilon_{eo}) + \sum_{i=1,2} 2\pi q R_i h_R \left(\int_0^{L_i} n dz \right) u_B (\varepsilon_c + \varepsilon_{ir} + \varepsilon_{er}). \quad (A7)$$

Here, ε_c are the collisional energy losses from ionization and excitation (cross-sections for Xenon are taken from Ref. 41), while ε_{ic} , ε_{io} , ε_{ir} , ε_{ec} , ε_{er} , ε_e , and ε_{eo} are kinetic energy losses at the thruster backwall, radial walls, and exit, respectively (see Ref. 31 for more details). The total thrust force (ignoring the thrust from the neutral gas) is then calculated using

$$F_p = \left(\frac{M_{det}^2 + 1}{2M_{det}} \right) F_0, \quad (A8)$$

where

$$F_0 = q\beta n_0 T_e A_0. \quad (A9)$$

¹C. Charles, *J. Phys. D: Appl. Phys.* **42**, 163001 (2009).

²J. S. Sovey, V. K. Rawlin, and M. J. Patterson, *J. Propul. Power* **17**, 517–526 (2001).

³H. Kuninaka, K. Nishiyama, I. Funaki, T. Yamada, Y. Shimizu, and J. Kawaguchi, *J. Propul. Power* **23**, 544–551 (2007).

⁴I. G. Mikellides, I. Katz, R. R. Hofer, D. M. Goebel *et al.*, *Phys. Plasmas* **18**, 033501 (2011).

⁵A. D. Gallimore and M. S. McDonald, *IEEE Trans. Plasma Sci.* **39**, 2952 (2011).

⁶R. E. Wirz and R. W. Conversano, *J. Spacecraft Rockets* **50**, 1035 (2013).

⁷A. Aanesland, S. Mazouffre, and P. Chabert, *Europhys. News* **42**(6), 28–31 (2011).

⁸D. Rafalskyi and A. Aanesland, *J. Phys. D: Appl. Phys.* **47**, 495203 (2014).

⁹A. V. Arefiev and B. N. Breizman, *Phys. Plasmas* **15**, 042109 (2008).

¹⁰K. Takahashi, T. Laffleur, C. Charles, P. Alexander *et al.*, *Appl. Phys. Lett.* **98**, 141503 (2011).

¹¹J. Navarro-Cavallé and E. Ahedo, *Phys. Plasmas* **20**, 043512 (2013).

¹²R. Geller, *Electron Cyclotron Resonance Ions Source and ECR Plasmas* (Institute of Physics Publishing, 1996).

¹³S. D. Leifer, J. J. Blandino, and J. C. Sercel, *AIP Proc.* **217**, 482 (1991).

¹⁴J. Navarro-Cavallé, E. Ahedo, M. Merino, V. Gomez, M. Ruiz, and J. A. Gonzalez del Amo, in *Proceedings of the 33th International Electric Propulsion Conference, Washington D. C., USA* (2013), p. 285.

¹⁵K. Takahashi, C. Charles, R. Boswell, and A. Ando, *J. Phys. D: Appl. Phys.* **46**, 352001 (2013).

¹⁶D. B. Miller and G. W. Bethke, *AIAA J.* **4**, 835–840 (1966).

¹⁷D. B. Miller and E. F. Gibbons, *AIAA J.* **2**, 35–41 (1964).

¹⁸M. Nagatomo, in *Proceedings of the Seventh International Symposium on Space Technology and Science, Tokyo, Japan, 1967*.

¹⁹G. H. Kosmahl, Cleveland, NASA, TN D-3782 (1967).

²⁰J. C. Sercel, Ph.D. thesis, “An experimental and theoretical study of the ecr plasma engine,” Pasadena, California Institute of Technology, 1993.

²¹D. M. Goebel and I. Katz, *Fundamental of Electric Propulsion, Ion and Hall Thrusters* (John Wiley & Sons, 2008).

²²R. Tang, Ph.D. thesis, “Study of the gasdynamic mirror (GDM) propulsion system,” University of Michigan, 2011.

²³A. V. Arefiev and B. N. Breizman, *Phys. Plasmas* **11**, 2942 (2004).

²⁴C. S. Olsen, M. G. Ballenger, M. D. Carter *et al.*, *IEEE Trans. Plasma Sci.* **43**(1), 252 (2015).

²⁵S. Larigaldie, U.S. patent 0,020,502 A1 (22 January 2015).

²⁶T. Takahashi, Y. Takao, K. Eriguchi, and K. Ono, *J. Phys. D: Appl. Phys.* **41**, 194005 (2008).

²⁷T. Takahashi, Y. Takao *et al.*, *Phys. Plasmas* **18**, 063505 (2011).

²⁸J. Jarrige, P. Q. Elias, F. Cannat, and D. Packan, “Characterization of a coaxial ECR plasma thruster,” AIAA Paper No. 2013–2628, 2013.

²⁹J. Jarrige, P. Q. Elias, F. Cannat, and D. Packan, in *Proceedings of the 33th International Electric Propulsion Conference, Washington D. C., USA, October 6–10* (2013), p. 420.

³⁰F. Cannat, J. Jarrige, P.-Q. Elias, and D. Packan, in *Proceedings of the Space Propulsion Conference, Cologne, Germany* (2014), paper no. 2014–2980728.

³¹T. Laffleur, *Phys. Plasmas* **21**, 043507 (2014).

³²W. Cox, C. Charles, R. W. Boswell, and R. Hawkins, *Appl. Phys. Lett.* **93**, 071505 (2008).

³³C. A. Deline, R. D. Bengtson, B. N. Breizman *et al.*, *Phys. Plasmas* **16**, 033502 (2009).

³⁴F. N. Gesto, B. D. Blackwell, C. Charles, and R. W. Boswell, *J. Propul. Power* **22**, 24 (2006).

³⁵M. Merino and E. Ahedo, *Plasma Sources Sci. Technol.* **23**, 032001 (2014).

³⁶A. Aanesland, J. Bredin, P. Chabert, and V. Godyak, *Appl. Phys. Lett.* **100**, 044102 (2012).

³⁷V. A. Godyak and V. I. Demidov, *J. Phys. D: Appl. Phys.* **44**, 233001 (2011).

³⁸A. Shabshelowitz and A. D. Gallimore, *J. Propul. Power* **29**, 919 (2013).

³⁹A. Aanesland, L. Liard, G. Leray, J. Jolly, and P. Chabert, *Appl. Phys. Lett.* **91**, 121502 (2007).

⁴⁰A. Fruchtman, K. Takahashi, C. Charles, and R. W. Boswell, *Phys. Plasmas* **19**, 033507 (2012).

⁴¹A. V. Phelps, *Compilation of Atomic and Molecular Data* (2008).



BP 72 - 29 avenue de la Division Leclerc - 92322 CHATILLON CEDEX - Tél. : +33 1 46 73 40 40 - Fax : +33 1 46 73 41 41

www.onera.fr